Laser Polarimetry of Birefringence of Architectonics of Biotissues

A.G. Ushenko[1], O.I.Olar[2], Yu.A. Ushenko[1]

[1]Chernivtsi National Uviversity, 2 Kotsyubinsky Str., 58012 Chernivtsi, Ukraine
[2]Bucovinian State Medical Academy, 2 Teatralna Sq., 58000 Chernivtsi, Ukraine
ushenko@itf.cv.ukrtel.net

Received 12.04.2003

Abstract

The features of polarization tomography of optically anisotropic architectonic nets of biotissues (BT) of different morphological structures have been investigated. The peculiarities of phase mapping of skin derma, muscular and bone BT have been experimentally studied. The interrelation between the PT structure and physiological state of BT has been determined. The criteria of early diagnostics of the appearance of degenerative-dystrophic and pathological changes in the structure of BT optically anisotropic architectonics have been revealed.

Keywords: polarimetry, birefringence, biotissues

PACS: 42.62Be, 42.81.Gs

1. Introduction

Light-based techniques are becoming an increasingly popular method for probing heavily scattering media such as body tissue [1,2,3,4]. For a surface tissue or thin tissue samples it is possible to use the coherence or polarization properties of the light [5–21].

Early works in the field of tissue optics have assumed a homogeneous scattering medium and measured the bulk scattering and absorption properties. More recently, attempts have been made to characterize the effect of different tissue layers. The problem of using the light to probe layered scattering media is that the scattered light propagates along many random paths through the different layers. It would be extremely useful to be able to characterize the optical properties and thickness of different layers from the measurements of properties of the emerging light. For example, in the studies of thick tissues, the models for the brain have been developed to include the effects of skin, bone, cerebrospinal fluid, as well as a white and grey matter.

Among the variety of directions of laser polarimetry (LP) of phase-inhomogeneous layers (PIL), the development of LP techniques in the optics of biotissues (BT) is promising.

It should be expected that the LP techniques will provide a new information about the morphological and optically anisotropic structure of BT on both micro- and macroscopic levels of their arrangement, which is urgent for optical diffuse and coherent tomography, directed towards visualization and obtaining images of macroinhomogeneities in BT (tumours, haematomas, etc.).

That is why it could be stated that optical tomography demands further developments both in determining the interrelation of orientation-phase structure of BT architectonics with their physiological state and in obtaining new types of

tomograms and their processing. Therefore, it would be expedient to elaborate techniques of BT polarization tomography, based on polarization selection of BT architectonic images with obtaining the set of orientational and phase tomograms.

Thus, the urgency of such a direction is stipulated by the necessity in a more detailed investigation of the structure of different types of PIL; elaboration of new approaches of LP towards the analysis and measuring the properties of their object fields; the search of new techniques (as well as improving the traditional ones) for the diagnostics of optical-geometric parameters of the PIL with surface and volumetric inhomogeneous constituents; visualization and reconstruction of phase-orientational structure of the BT architectonics.

2. The objects of investigation

The following types of BT were used as the objects of investigation: skin derma (SD), muscular tissue (MT) and bone tissue (BnT). These objects were chosen according to their common optical features of architectonics – spatial nets, the substance of which possesses the features of optically uniaxial crystals [22–24]. But there are also some differences.

The SD architectonics[22] is formed by statistically oriented beams (Fig. 1) of collagen fibrillae (the value of birefringence being $\Delta n \approx 10^{-3}$). The4 diameter of the fibrillae ranges from 0.5 to 2 μm. The parallel beams of fibrillae form a fibre, whose diameter changes from 100 to 200 μm.

The BnT architectonics represents a system [23] consisting of the layer of trabeculae and osteons (Fig. 2). The optically active matrix is formed by the hydroxylapathite crystals ($\Delta n \approx 10^{-1}$), long (optical) axes of which are oriented along the longitudinal axis of collagen fibres. They are situated between the microfibrillae, fibrillae and collagen fibres, forming the independent continuous phase.

MT is a structurized spatially ordered system of protein beams (Fig. 3), consisting of optically isotropic actine and anisotropic ($\Delta n \approx 10^{-3}$) miosine [24].

The totality of bioobjects chosen for investigation covers completely the variety of orientation-phase structure of the BT architectonic nets. This can be regarded as the basis of diagnostics for the transformation processes of morphological structure of the other types of BT, e.g., the soft tissues of women's reproductive sphere.

3. Theoretical modelling

Optical properties specified by a crystalline structure of the architectonics of morphologically different BTs are adequately described by the following Jones operator [25] :

$$\{M\} = \begin{Vmatrix} \cos^2\rho(X,Y) + \sin^2\rho(X,Y)\exp\left[-i\delta(X,Y)\right] & \cos\rho(X,Y)\sin\rho(X,Y)\left\{1-\exp\left[-i\delta(X,Y)\right]\right\} \\ \cos\rho(X,Y)\sin\rho(X,Y)\left\{1-\exp\left[-i\delta(X,Y)\right]\right\} & \sin^2\rho(X,Y) + \cos^2\rho(X,Y)\exp\left[-i\delta(X,Y)\right] \end{Vmatrix} \quad (1)$$

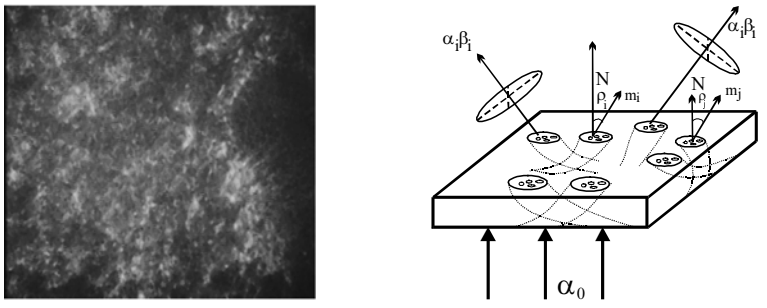

a) b)

Fig. 1. Microphotograph (a) and model representation (b) of skin derma architectonics. ρ - orientational parameters of architectonics; α_i, α_j –azimuth and β_i, β_j – ellipticity of emergent light, α_0 - the polarization azimuth of the laser beam, m_i,m_j - fibrillate directions.

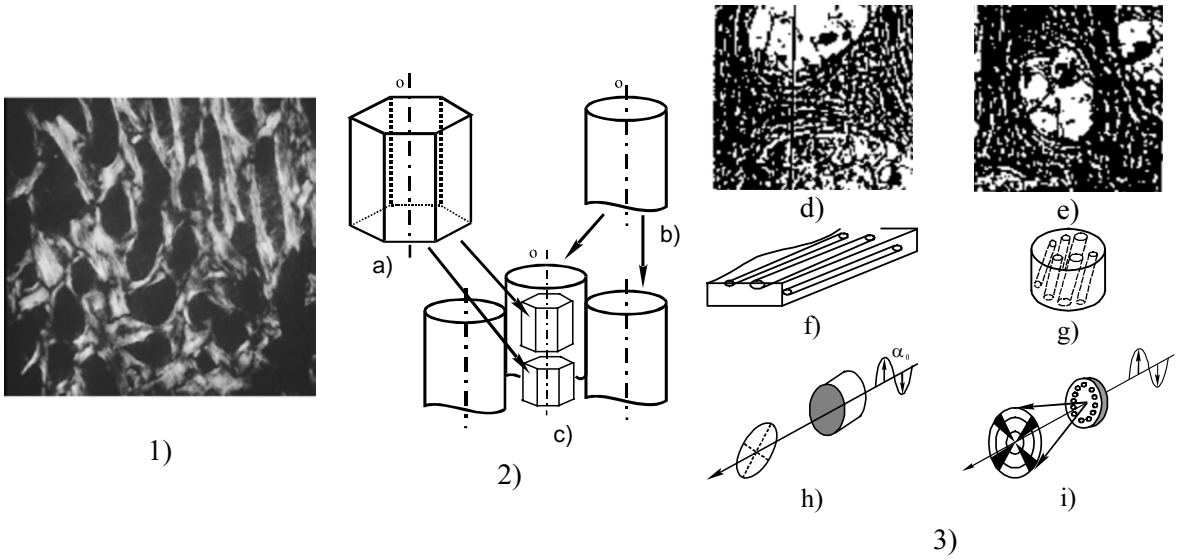

Fig. 2. Microphotograph (1), model representation of bone tissue structure (2) and light propagation through bone tissue (3): trabeculae (a), osteons (b) and theirpacking (c); microphotographs at light propagation perpendicular (d) and along (e) osteons, respectively; osteons packing shematical representation (f,g); emergent light elliptisity (h) and conoscopic fringes (i).

where $\rho(X,Y)$ and $\delta(X,Y)$ are, respectively, the orientational (the direction of fibrillate packing) and the phase (the fibrillate substance birefringence) parameters of the BT architectonics.

The coordinate (X,Y) relation of these parameters leads to the fact that the architectonics image appears to be inhomogeneous with respect to polarization and is the combination of local zones, whose state of polarization (azimuth α and ellipticity β) is determined by the relations [26]

$$\alpha(X,Y)=0.5\arctan\left[\frac{\sin 2\rho\cos 2\rho(1-\cos\delta)\cos 2\alpha_0+(\sin^2 2\rho+\cos^2 2\rho\cos\delta)\sin 2\alpha_0}{(\cos^2 2\rho+\sin^2 2\rho\cos\delta)\cos 2\alpha_0+\sin 2\rho\cos 2\rho(1-\cos\delta)\sin 2\alpha_0}\right], \quad (2)$$

$$\beta(X,Y)=0.5\arcsin[\sin 2(\rho-\alpha_0)\sin\delta]. \quad (3)$$

Here α_0 denotes the polarization azimuth of the laser beam (with the wavelength λ) illuminating the BT.

It can be seen from the analysis of (2) and (3) that the intensity of every point $I(X,Y)$ of the architectonics image of the BT sample with the geometric thickness L is determined by both the orientation of optical axes of fractal domains and the optical anisotropy of its substance $\Delta n(X,Y)=\delta[(2\pi/\lambda)L]^{-1}$.

Such the dependence can be determined analytically by solving the matrix equation, which is written for the conditions of crossed transmission axes of polarizer and analyser and the illumination with a linearly polarized laser beam with the azimuth $\alpha_0=0^0$.

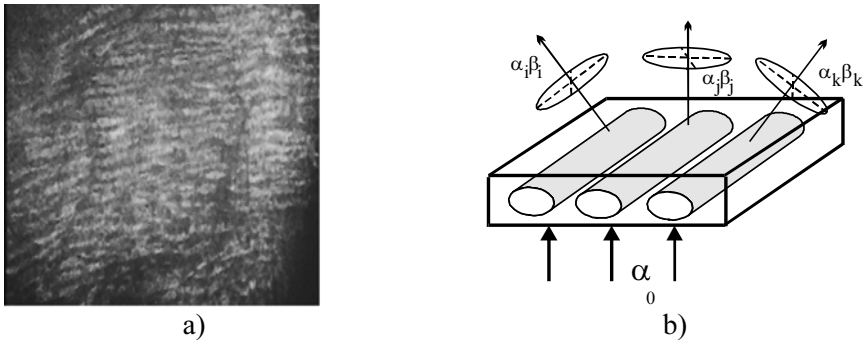

Fig. 3. Microphotograph (a) and model representation (b) of muscle tissue structure: $\alpha_i, \alpha_j, \alpha_k$ –azimuth and β_i, β_j, β_k – ellipticity of emergent light, α_0 - the polarization azimuth of the laser beam.

$$U(X,Y)=0.25\{A\}\{\mathrm{M}\}\{P\}D_0=0.25\begin{Vmatrix}1 & -1\\ -1 & 1\end{Vmatrix}\times$$
$$\times\begin{Vmatrix}\cos^2\rho(X,Y)+\sin^2\rho(X,Y)\exp[-i\delta(X,Y)] & \cos\rho(X,Y)\sin\rho(X,Y)\{1-\exp[-i\delta(X,Y)]\}\\ \cos\rho(X,Y)\sin\rho(X,Y)\{1-\exp[-i\delta(X,Y)]\} & \sin^2\rho(X,Y)+\cos^2\rho(X,Y)\exp[-i\delta(X,Y)]\end{Vmatrix}\times\times\begin{Vmatrix}1 & 1\\ 1 & 1\end{Vmatrix}\begin{pmatrix}1\\ 1\end{pmatrix} \quad (4)$$

Here D_0, $U(X,Y)$ are the Jones vectors of illuminating and object laser beams, respectively, $\{A\}$, $\{M\}$ and $\{P\}$ the Jones matrices of analyser, object and polarizer, respectively, and X and Y the coordinates in the plane of BT sample.

After the multiplication we obtain

$$U(X,Y)=0.5\cos 2\rho(X,Y)\left\{1-e^{-i\delta(x,y)}\right\}\begin{pmatrix}1\\ -1\end{pmatrix} \quad (5)$$

From (5) we get the object field intensity in the form

$$I(X,Y)=U(X,Y)U^{\otimes}(X,Y)=$$
$$=I_0\cos^2 2\rho(X,Y)\sin^2\left[\delta(X,Y)/2\right], \quad (6)$$

where I_o is the intensity of the illuminating laser beam.

It follows from (6) that the lines of zero intensity ("polarizophotes") due to the orientation of optical axes in crystallite domains, which coincide with the polarization azimuth of the illuminating laser beam $I^*_\rho(X,Y)=0|\alpha_0=\rho$, can be found in the visualized BT architectonics image. This ensures the possibility of polarization selection of the information in such the image – the determination of totality of equally oriented anisotropic domains.

Indeed, by means of rotating simultaneously the transmission axes of the crossed polarizers, one can obtain the series of orientational tomograms of BT architectonics in the form of topological distribution of polarizophotes $I^*_\rho(X,Y,\omega)=0|\alpha_0(\omega)=\rho(\omega)$, where ω is the rotation angle.

On the other hand, the information about the anisotropy of the BT architectonic net substance remains to be vague.

For determining the phase constituent in the coherent BT image it is necessary to place the sample into the polarization system, consisting of two crossed phase filters – quarter-wave plates - and the polarizers, of which the transmission axes make the angles +45° and –45° with the slow and fast axes, respectively.

In this case the coordinate distribution of the intensity $I_\delta(X,Y)$ is determined by the Jones vector of the object field $E(X,Y)$, which may be found by means of solving the following matrix equation:

$$E(X,Y)=0.25\{A\}\{\Phi_2\}\{\mathrm{M}\}\{\Phi_1\}\{P\}D_0=0.25\begin{Vmatrix}1 & -1\\ -1 & 1\end{Vmatrix}\begin{Vmatrix}i & 0\\ 0 & 1\end{Vmatrix}\times$$
$$\times\begin{Vmatrix}\cos^2\rho(X,Y)+\sin^2\rho(X,Y)\exp[-i\delta(X,Y)] & \cos\rho(X,Y)\sin\rho(X,Y)\{1-\exp[-i\delta(X,Y)]\}\\ \cos\rho(X,Y)\sin\rho(X,Y)\{1-\exp[-i\delta(X,Y)]\} & \sin^2\rho(X,Y)+\cos^2\rho(X,Y)\exp[-i\delta(X,Y)]\end{Vmatrix}\times \quad (7)$$
$$\times\begin{Vmatrix}1 & 0\\ 0 & i\end{Vmatrix}\begin{Vmatrix}1 & 1\\ 1 & 1\end{Vmatrix}\begin{pmatrix}1\\ 1\end{pmatrix}$$

Here $\{\Phi_1\}$, $\{\Phi_2\}$ are the Jones matrices of the quarter-wave plates and $\{A\}$ and $\{P\}$ the Jones matrices of the analyser and polarizer, respectively.

The solution of (7) is the Jones vector of the object field,

$$E(X,Y)=0.5\begin{pmatrix}\{-Q(1-\nu)-G\eta\}+i\{G(1-\nu)-Q\eta\}\\ \{Q(1-\nu)+G\eta\}+i\{-G(1-\nu)+Q\eta\}\end{pmatrix}, \quad (8)$$

where

$$Q=\cos 2\rho(X,Y);\ G=\sin 2\rho(X,Y);$$
$$\nu=\cos\delta(X,Y);\ \eta=\sin\delta(X,Y). \quad (9)$$

It follows from (8) and (9) that the coordinate distribution of the intensities of BT's phase maps appear to be unambiguously related to the optical anisotropy of its substance by the following relation:

$$I_\delta(X,Y) = E(X,Y)E^{\otimes}(X,Y) = \\ = I_0 \sin^2\left[\delta(X,Y)/2\right] \quad . \qquad (10)$$

Thus, the described approach provides the information about the birefringence of BT architectonics substance, irrespective of the directions of packing of its optically anisotropic fibrillae.

4. Automatic polarimeter design

The overall layout of the instrument is shown in Fig. 4. The main optical elements of the polarimeter are the He-Ne laser (λ = 0.6328 μm, 10 mW), the polaroid P, the two quartz-made quarter-wave ($\lambda/4$) plates (of the fourth order) and the analyser polaroid A. By setting the polarization plane of P parallel to the optical axis of the first quarter-wave plate, the object O under test (a tissue sample) is illuminated by a linearly polarized light beam.

The He-Ne laser beam is expanded by the afocal system R up to the diameter of 3 mm. The pinhole located in the expansion optics removes the scattered light originating from secondary reflections in the resonator and optics contaminations. The role of the half-wave plate $\lambda/2$ is to match the laser beam polarization plane to the polarizer transmittance direction and, at the same time, control the light intensity level at the CCD matrix to avoid its saturation.

The tissue sample is placed at the microscope slide. The slide with tissue is fixed in a mount, providing transverse translations in the two mutually perpendicular directions within the range of 5 mm, in order to enable choosing various fragments of the sample.

The sample image is formed at the CCD matrix by the optical system composed of two microscope objectives. The overall dimensions of the quarter-wave and analyser-driving systems do not allow to place the imaging optics closer than 200 mm from the sample. The images registered by the CCD matrix and the frame grabber are transferred in a digital form to the computer memory.

The half-wave plate, the two quarter-wave plates, the polarizer and analyser are rotated by means of step motors. One motor step corresponds to the rotation of the optical element by 22.5 minutes of arc.

Before making measurements, the automatic system calibration is performed in the following order:

1. The optical axes of the quarter-wave plates are set parallel to the transmittance directions of polarizers;
2. The transmittance planes of polarizer and analyser are set parallel;
3. The half-wave plate is rotated to obtain the

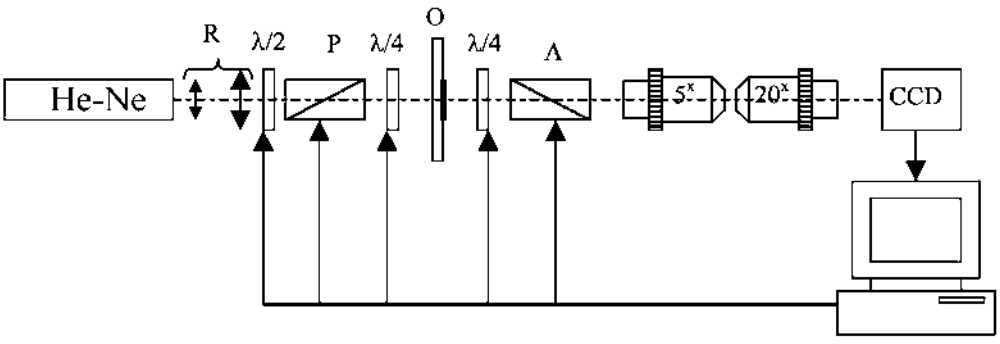

Fig. 4. Optical scheme. (explanations in the text)

maximum signal level registered by the CCD matrix (without saturation);

4. Both the analyser and the second quarter-wave plate are rotated to the crossed position with the polarizer.

5. Experimental results and discussion

The following types of morphological sections of biotissues were used as the objects under investigation:

- bone tissue (the refraction coefficient μ_a = 2.63 cm^{-1}; the scattering coefficient μ_s = 60.02 cm^{-1}, the anisotropy parameter g = 0.88, the birefringence Δn = 0.1, the geometric thickness z = 40 μm);
- skin derma (μ_a = 2.2 cm^{-1}, μ_s = 185 cm^{-1}, g = 0.82, Δn = 0.01, z = 30 μm);
- fibrillar muscular tissue (μ_a = 2 cm^{-1}, μ_s = 215 cm^{-1}, g = 0.96, Δn=0.03, z = 30 μm).

The histological sections of BTs were made for the experiment, the geometric thickness L of which satisfied the condition of single scattering (the attenuation index τ<0,1) and was 100 μm for SD, 70 μm for MT and 50 μm for Bnt, respectively.

Fig. 5 shows the series of maps visualizing the totalities of polarizophotes $I^*_\rho(X,Y)=0|\alpha_0=\rho$ in the coherent BnT image.

The rotation range of the crossed axes of polarizer and analyser amounted 0° – 90° with the step of $\omega = 1^0$.

It can be seen from the data that the polarization selection of the object field enables to gain the images of BnT as the topological distributions of polarizophotes (Fig. 5a ($\omega = 0^0$), Fig. 5b ($\omega = 45^0$) and fig. 5c ($\omega = 55^0$)) of the packing directions of collagen mineralized fibres.

At the same time, the curvilinear architectonics of the fibrillae, characteristic of BnT osteons (the marked out rectangular fragments in Fig. 5), restricts the capability of orientational tomography for the situation, in which optically anisotropic fibrillae are oriented at a non-zero angle with respect to the plane of the sample under study.

Indeed, when the direction of the biocrystals' optical axis changes continuously, a specific local state of polarization is formed in every point of the object field [25]. The similar structure of Bnt architectonics manifested itself in the fact that the rotation angle ω variants of the crossed polarizers do not practically affect the topological distribution of polarizophotes of the BnT image. This fact points to the necessity of obtaining additional information about the phase structure of the BT architectonics, connected with the value of its substance birefringence.

On the other hand, this information is urgent for estimating the BnT architectonics trabeculae orientational structure, which is related to the diagnostics of its physiological state [27].

The distributions of birefringence $\Delta n(X,Y)$ of the architectonics substance of SD, MT and BnT are presented in Fig. 6, from which the following can be seen:

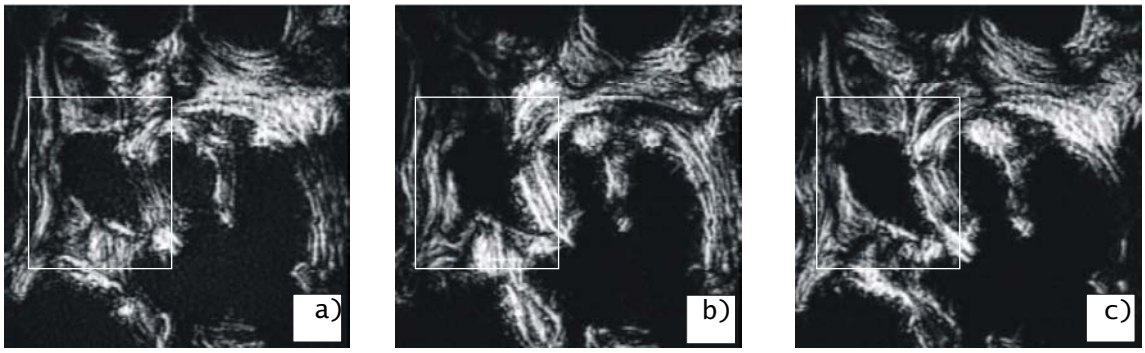

Fig. 5. Polarization maps of bone tissue architectonics.

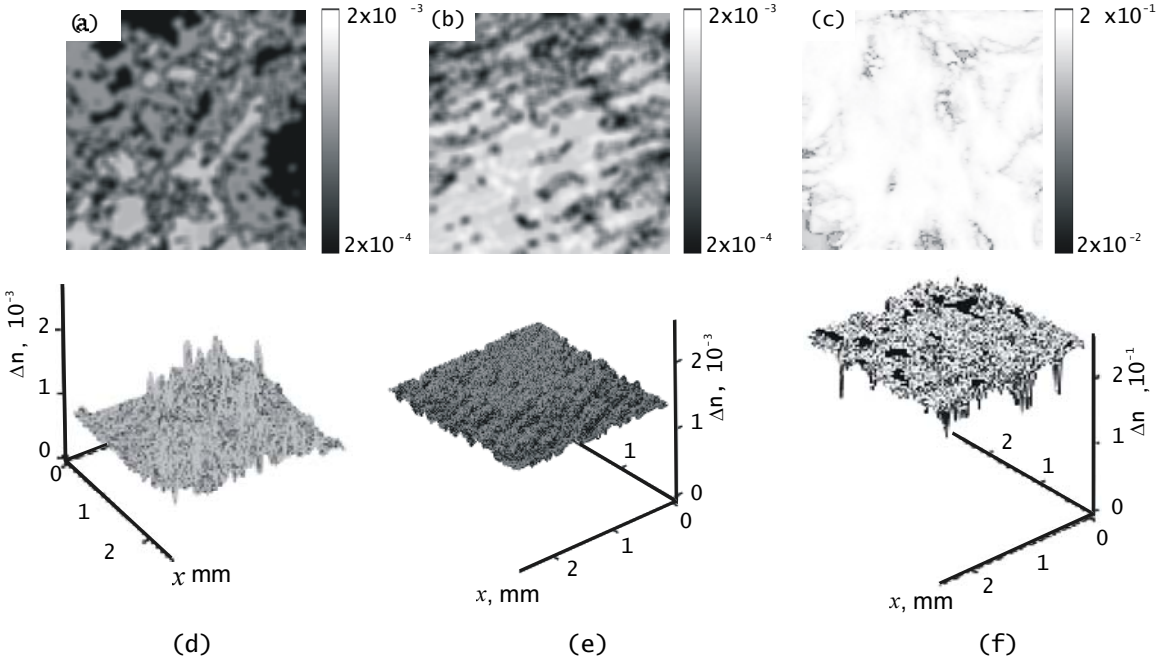

Fig. 6. Phase maps of skin derma (a,d), muscular tissue (b,e) and bone tissue (c,f) (explanations in the text)

1. The topological distribution of the $\Delta n(X,Y)$ parameter in the areas of localization of collagen bundles of SD (irrespective of their orientation in the sample's plane) is rather homogeneous (Fig. 6a). The level of optical anisotropy of SD architectonics net ranges within the limits $\Delta n(X,Y) \approx 0{,}5\times10^{-3} \sim 1{,}5\times10^{-3}$ (Fig 6d). This satisfies the data for the collagen protein birefringence described in [1,2].

2. The high orientational order of the optical anisotropy zones ($\Delta n(X,Y) \neq 0$) due to the specifics of angular structure of the MT architectonics is a characteristic topological peculiarity of MT phase maps (Fig. 6b). The MT phase maps represents a quasi-periodical distribution of birefringence $\Delta n(X,Y)$ (Fig. 6e) of the miosine bundle substance, whose value practically coincides with the data obtained for the collagen structures (Fig. 6a).

3. The phase-shifting ability of the BnT sample is two orders of magnitude higher (Fig. 6c) in comparison with the anisotropy of collagen and miosine nets ($\Delta n(X,Y) \approx 0{,}7\times10^{-1} \sim 1{,}5\times10^{-1}$ (Fig 6f). Such a peculiarity is associated with the level of birefringence in hydroxylapathite crystals.

5. Diagnostics of degenerative-dystrophic and pathological changes in BT architectonics

The appearance of pathological and degenerative-dystrophic processes in the BTs at the early (pre-clinic) stages is accompanied by the following morphological changes [27-29] of their architectonics:

- decrease in the mineral substance concentration and disorientation of the BnT architectonic net (rachitis, osteoporosis, etc.);
- excrescence of the collagen structures liming the soft tissues (psoriasis, calcinosis, myoma, fibromyoma).

From the viewpoint of optics, the tendencies to such changes in the first case can be determined as $\Delta n \rightarrow \Delta n_{min}$ and, in the limit, $\Delta n \rightarrow 0$. In the second case we should have $\Delta n \rightarrow \Delta n_{max}$.

The appearance of such the processes can be analytically estimated by finding the second statistical moment of the random intensity distribution $\Omega_{I(X,Y)}$ of phase maps of the BT's architectonics visualized via polarization:

$$\Omega_{I(X,Y)} = \left\langle I_\delta{}^2(X,Y) - \left\langle I_\delta{}^2(X,Y) \right\rangle \right\rangle, \qquad (11)$$

where $I_\delta(X,Y)$ and $\langle I_\delta(X,Y)\rangle$ are, respectively, the random and the mean values of the intensities of phase maps of the BT architectonics.

On the other hand, during the polarization selection of information, the value of intensities at every point of phase maps is determined by the polarization (α, β) features of the BT image, the values of which are distributed in accordance with the probability densities Q_α and U_β:

$$I_\delta(X,Y) = \\ = I_0 \int\limits_\alpha \int\limits_\beta Q_\alpha U_\beta \begin{bmatrix} \cos^2(\alpha-\Theta)+ \\ +\tan^2\beta \sin^2(\alpha-\Theta) \end{bmatrix} d\alpha d\beta . \quad (12)$$

Thus, the local value of birefringence $\Delta n(X,Y)$ at every point of the obtained phase maps appears to be connected with the polarization structure of BT architectonics image by the following relation:

$$\Delta n(X,Y) = \frac{\lambda}{\pi L}\arcsin\times \\ \times\sqrt{\int\limits_\alpha \int\limits_\beta Q_\alpha U_\beta \begin{bmatrix} \cos^2(\alpha-\Theta)+ \\ +\tan^2\beta \sin^2(\alpha-\Theta) \end{bmatrix} d\alpha d\beta} . \quad (13)$$

Consequently, while measuring the intensity dispersion $\Omega_{I(X,Y)}$ of the phase maps, one can unambiguously determine the birefringence dispersion $\Omega_{\Delta n(X,Y)}$, which is a statistic estimation of physiological state of the BT architectonics,

$$\Omega_{\Delta n(X,Y)} = \left\langle \Delta n^2(X,Y) - \left\langle \Delta n^2(X,Y) \right\rangle \right\rangle . \quad (14)$$

The results illustrating the possibilities of polarization-phase tomography in pre-clinic diagnostics of degenerative-dystrophic changes of the BT are presented in Fig. 7.

In the left-hand column, the phase maps of physiologically normal (Fig. 7a) and degeneratively changed (Fig. 7d) trabeculae (quasi-plane trabecula) of the BnT architectonics are given. The central (Fig. 7b, e) and the right (Fig. 7c,f) columns correspond to non-uniformly scaled topological distributions of the birefringence value $\Delta n(X,Y)$.

It can be seen from the obtained data that for physiologically normal sample of bone plate the topology (Fig. 7a) and the value (Fig. 7b, c) of birefringence $\Delta n(X,Y)$ of the architectonics substance are practically homogeneous within the areas of its fractal domains (40 – 200 μm). The structure of phase maps of the BnT sample with the probability of osteoporosis appearance [27-29] (architectonics ecalcination) is quite different. As it is shown in Fig. 7 d, e, f, the topological distribution $\Delta n(X,Y)$ is transformed into the set of small-scale (5-30 μm) areas (Fig. 7d). The anisotropy level of BnT architectonics decreases by an order ($\Delta n(X,Y) \approx 0{,}2\times10^{-2}$ ~$1{,}2\times10^{-2}$, see Fig. 7e). The downward excursion of the birefringence value $\Delta n(X,Y)$ of the architectonics substance for degeneratively changed sample of the BnT then occurs (Fig. 7f). The statistics of such changes is illustrated by the series of diagrams of changes in dispersion fluctuations $\Delta n(X,Y)$ obtained for the BnT phase maps (Fig. 7g). The experiments data obtained for physiologically normal BnT (continuous columns – 30 samples) and degeneratively changed (the shaded columns – 28 samples).

The comparative analysis of the obtained diagrams proves that they practically do not overlap within the limits of statistically reliable groups of the samples under study. That is why it is possible to suggest the application of this statistic parameter of BT architectonics phase maps in early diagnostics of its degenerative-dystrophic changes.

Pathological change (intumescence and excrescence of the fibres) of architectonics of soft tissue collagen net by the example of women's reproductive sphere BT (myometry) [29] is illustrated by the series of phase maps presented in Fig. 8. In the left column the phase maps of physiologically normal (Fig. 8a) and pathologically changed samples of myometry – diffuse transformation (myoma) of architectonics (Fig. 4c), as well as forming of the fibromyoma growth direction (Fig. 8e), are presented. In the right-hand corner the

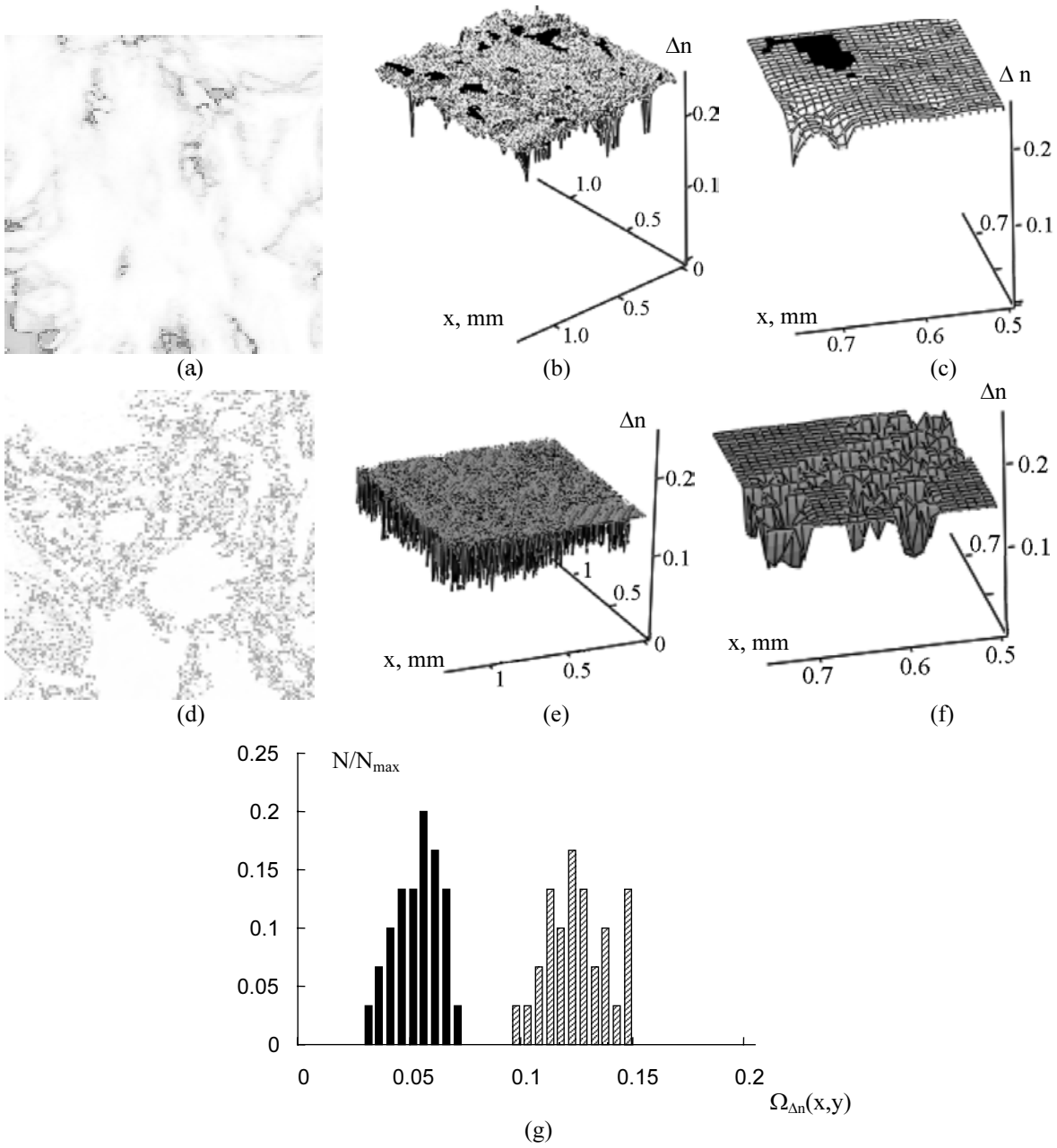

Fig. 7. Diagnostics of degenerative-dystrophic changes of bone tissue. (explanations in the text)

coordinate distributions of the collagen fibre birefringence value are presented (Fig. 8b, d, f).

From the data obtained above we can find out the following:

1. Optical anisotropy of physiologically normal myometry is not practically apparent – the phase maps represent a quasi-homogeneous field (Fig. 3a) with several fluctuations $\Delta n(X,Y) \approx 10^{-5}$ (Fig. 8b). This points to a rather amorphous optical structure of BT, i.e., to "lack of development" of myometry collagen net.
2. The topology of phase component of the diffusely changed myometry architectonics if formed by the areas with inhomogeneous distribution (Fig. 8c, d) of birefringence $\Delta n(X,Y)$, the values of which vary from 1.2×10^{-4} to 1.1×10^{-3}, respectively.
3. The tumour-forming processes are accompanied by the formation of "anisotropy zones" (Fig. 7e), within which the birefringence value of architectonics

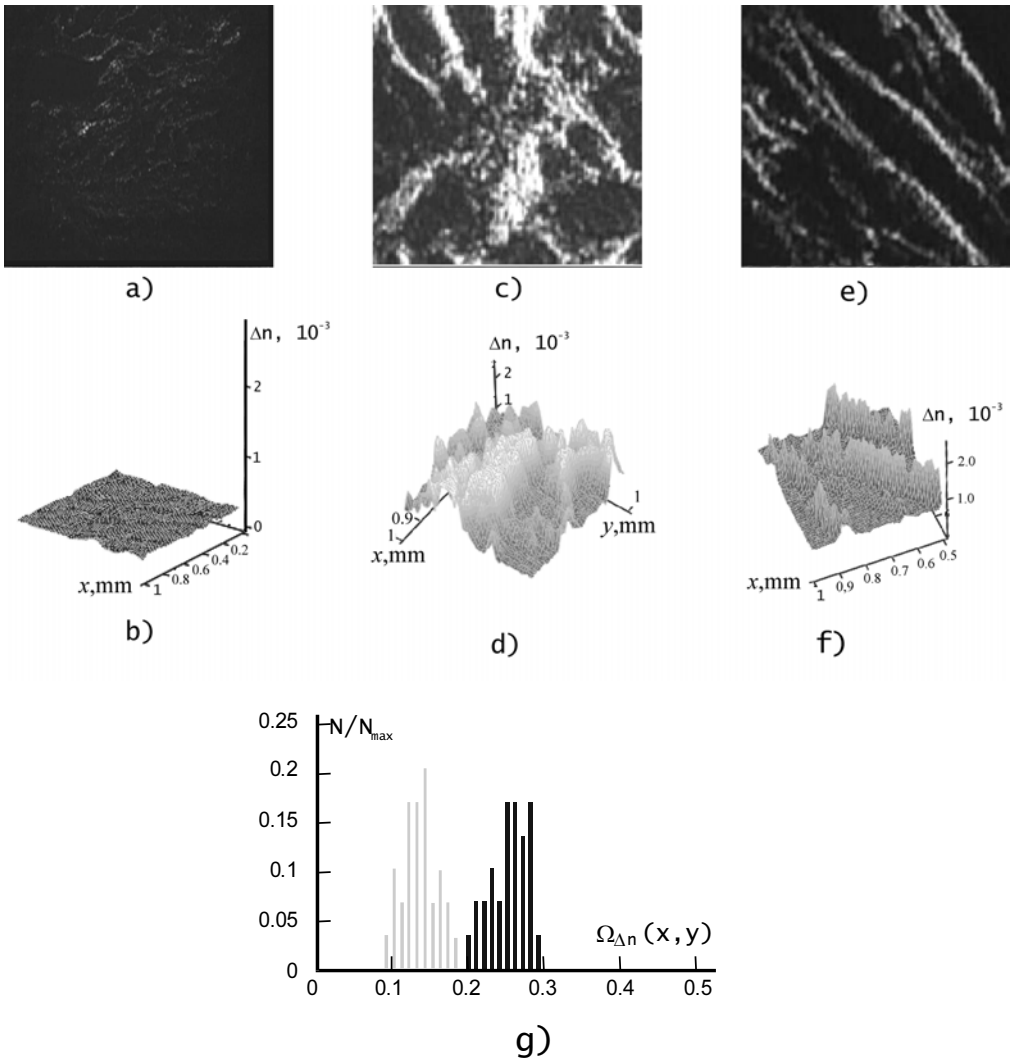

Fig.8. Diagnostics of pathological changes in myometry collagen net (explanations in the text)

increases by two orders of magnitude and reaches the level of 2.5×10^{-3} (Fig. 7f).

4. The statistics of experimental data obtained for physiologically normal (continuous columns – 42 samples) and pathologically changed (shaded columns – 39 samples) of the myometry tissues is illustrated by the diagrams of dispersion change $\Omega_{\Delta n(X,Y)}$ (Fig. 7g).

Our results testify that, within the investigated groups of samples, there is practically no overlapping of the parameters $\Omega_{\Delta n(X,Y)}$ of phase maps of the diagnosed BT architectonics. It points to diagnostic effectiveness of phase tomography in revealing pathological changes in its architectonics.

References

1. W.-F.Cheong, S.A.Prahl, and A.J.Welch, IEEE J. Quantum Electr., **26** (1989) p 2166.
2. R.R.Anderson, J.A.Parrish, "Optical properties of human skin" The Science of Photomedicine / Eds. Regan J.D., Parrish J.A. - N.Y.: Plenum Press, (1982)
3. V.V.Tuchin, Laser Physics, **8** (1998) p.1.
4. J.T.Bruulsema, J.E.Hayward, and T.J.Farrell, Opt. Lett., **22** (1997), p.190.
5. J.M.Schmitt, A.H.Gandjbakhche, and R.F.Bonnar, Appl. Opt., **31** (1992) p.6535.
6. H.Rinneberg, "Scattering of laser light in turbid media, optical tomography for medical diagnostics", The Inverse Problem /Ed. H.Lubbig.,Berlin, Akademie Verlag, pp. 107-

141, (1995).
7. D.A.Zimnyakov, V.V.Tuchin, and A.A.Mishin, Appl.Opt., **36** (1997) p.5594.
8. S.P.Morgan, M.P.Khong, and M.G.Somekh, Appl. Opt., **36** (1997) p.1560.
9. H.Horinaka, K.Hashimoto, K.Wada, and Y.Cho, Opt. Lett., **20** (1995).
10. M.R.Ostermeyer, D.V.Stephens, L.Wang, and S.L.Jacques, OSA TOPS on Biomedical Optics Spectroscopy and Diagnostics, OSA, Washington, **3** (1996) p.20.
11. A.M.Hielscher, J.R.Mourant, and I.J.Bigio, "Influence of particle size and concentration on the diffuse backscattering of polarized light," OSA TOPS on Biomedical Optics Spectroscopy and Diagnostics, OSA, Washington, **3** (1996) p.26.
12. D.Bicout, C.Brosseau, A.S.Martinez, and J.M.Schmitt, Phys. Rev.E., **49** (1994) p.1767.
13. J.R.de Boer, T.E.Milner, M.J.C.van Gemert, and J.S.Nelson, Opt. Lett., **22**,(1997) p. 934.
14. V.V.Tuchin, "Coherent and polarimetric optical technologies for the analysis of tissue structure (Overview)," Coherence-domain methods in biomedical science and clinical applications, Eds V.V.Tuchin, H.Podbielska, B.Ovryn. Bellingham, SPIE, **2981** (1997) p.120.
15. D.A.Zimnyakov, V.V.Tuchin, and K.V.Larin, "Speckle patterns polarization analysis as on approach to turbid tissues structure monitoring," Coherence-domain methods in biomedical science and clinical applications, Eds V.V.Tuchin, H.Podbielska, B.Ovryn. Bellingham, SPIE, **2981** (1997) p.172.
16. P.Bruscaglioni, G.Zaccanti, and Q.Wci, Opt., **32** (1993) p.6142.
17. I.Freund, M.Kaveh, R.Berkovits, and M.Rosenbluh, Phys.Rev.B., **42** (1990) p. 2613.
18. M.R.Hee, D.Huang, E.A.Swanson, and J.G.Fujimoto, J. Opt. Soc. Am. B., **9** (1992) p. 903.
19. H.-J.Schnorrenberg, M.Hengstebeck, K.Schlinkmeier, and W.Zinth, Proc. SPIE., Bellingham, SPIE, **2326-25** (1995); H.-J.Schnorrenberg, R.Habner, M.Hengstebeck et al. Proc. SPIE, Bellingham. SPIE, **2326-68**, (1995).
20. N.Kollias, Polarized light photography of human skin. In Bioengineering of the skin: skin surface imaging and analysis, Eds. K.-P.Wilhelm, P.Elsner, E.Berardesca, H.I.Maibach. Boca Raton et. al., CRC Press., (1997) pp.95-106, .
21. S.G.Demos, R.R.Alfano, Appl. Opt., (1997) p. 150.
22. A.G.Ushenko, V.P.Pishak, Proc.SPIE, **3317** (1997) p.418.
23. A.G.Ushenko, V.P.Pishak, "Crystal optic Properties of the transversy and longetudial sections of the bone," Proc.SPIE, **3317** (1997) p.425.
24. O.V.Angelsky, A.G.Ushenko, A.D.Arkhelyuk, and S.B.Yermolenko, Proc. SPIE, **3573** (1998) p.616.
25. A.G.Ushenko, "Laser diagnostics of biofractals," Quantum Electronics, **29** (1999) p.1078.
26. A.G.Ushenko, Laser Physics, **10** (2000) p.1.
27. O.V.Angelsky, A.G.Ushenko, D.N.Burkovets, V.P.Pishak, Yu.A.Ushenko, and O.V.Pishak, Laser Physics, **10** (2000) p. 1136.
28. A.G.Ushenko, Laser Physics, **10** (2000) p.1143 .
29. O.V.Angelsky, A.G.Ushenko, S.B. Ermolenko, D.N.Burcovets, and Yu.A.Ushenko, **89** (2000) p.973.